ACCOUNTS of chemical research

Article

pubs.acs.org/accounts

Enzyme Dynamics from NMR Spectroscopy

Published as part of the Accounts of Chemical Research special issue "Protein Motion in Catalysis".

Arthur G. Palmer, III*

Department of Biochemistry and Molecular Biophysics, Columbia University, 701 West 168th Street, New York, New York 10032, United States

CONSPECTUS: Biological activities of enzymes, including regulation or coordination of mechanistic stages preceding or following the chemical step, may depend upon kinetic or equilibrium changes in protein conformations. Exchange of more open or flexible conformational states with more closed or constrained states can influence inhibition, allosteric regulation, substrate recognition, formation of the Michaelis complex, side reactions, and product release. NMR spectroscopy has long been applied to the study of conformational dynamic processes in enzymes because these phenomena can be characterized over multiple time scales with atomic site resolution. Laboratory-frame spin-relaxation measurements, sensitive to reorientational motions on picosecond−nanosecond time scales, and rotating-frame relaxation-dispersion measurements, sensitive to chemical exchange processes on microsecond−millisecond time scales, provide information on both conformational distributions and kinetics. This Account reviews NMR spin relaxation studies of the enzymes ribonuclease HI from mesophilic (*Escherichia coli*) and thermophilic (*Thermus thermophilus*) bacteria, *E. coli* AlkB, and *Saccharomyces cerevisiae* triosephosphate isomerase to illustrate the contributions of conformational flexibility and dynamics to diverse steps in enzyme mechanism.

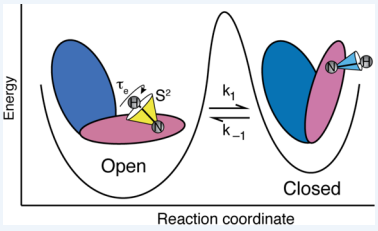

Spin relaxation measurements and molecular dynamics (MD) simulations of the bacterial ribonuclease H enzymes show that the handle region, one of three loop regions that interact with substrates, interconverts between two conformations. Comparison of these conformations with the structure of the complex between *Homo sapiens* ribonuclease H and a DNA:RNA substrate suggests that the more closed state is inhibitory to binding. The large population of the closed conformation in *T. thermophilus* ribonuclease H contributes to the increased Michaelis constant compared with the *E. coli* enzyme. NMR spin relaxation and fluorescence spectroscopy have characterized a conformational transition in AlkB between an open state, in which the side chains of methionine residues in the active site are disordered, and a closed state, in which these residues are ordered. The open state is highly populated in the AlkB/Zn(II) complex, and the closed state is highly populated in the AlkB/Zn(II)/2OG/substrate complex, in which 2OG is the 2-oxoglutarate cosubstrate and the substrate is a methylated DNA oligonucleotide. The equilibrium is shifted to approximately equal populations of the two conformations in the AlkB/Zn(II)/2OG complex. The conformational shift induced by 2OG ensures that 2OG binds to AlkB/Zn(II) prior to the substrate. In addition, the opening rate of the closed conformation limits premature release of substrate, preventing generation of toxic side products by reaction with water. Closure of active site loop 6 in triosephosphate isomerase is critical for forming the Michaelis complex, but reopening of the loop after the reaction is (partially) rate limiting. NMR spin relaxation and MD simulations of triosephosphate isomerase in complex with glycerol 3-phosphate demonstrate that closure of loop 6 is a highly correlated rigid-body motion. The MD simulations also indicate that motions of Gly173 in the most flexible region of loop 6 contribute to opening of the active site loop for product release. Considered together, these three enzyme systems illustrate the power of NMR spin relaxation investigations in providing global insights into the role of conformational dynamic processes in the mechanisms of enzymes from initial activation to final product release.

INTRODUCTION

Dramatic increases in the rates of chemical transformation by enzymes, compared with the uncatalyzed reactions in solution, result primarily from reductions in activation barriers within enzyme active sites. However, enzyme reaction mechanisms include other steps that have important consequences in determining efficacy. A simplified enzymatic reaction scheme is shown in eq 1, in which E′ represents one or more inactive states of the enzyme, E is the conformation of the enzyme competent for binding substrate, I is an inhibitor or transition-state analog, S_1 and S_2 are substrates or cofactors, which may bind in random or ordered (upper branch) fashion, the asterisk

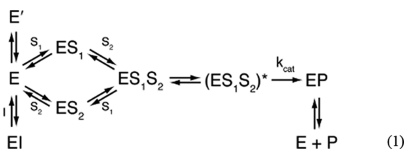

(1)

denotes the catalytically competent enzyme−substrate Michaelis complex, P is the product, and k_{cat} is the catalytic rate constant. Kinetic rate constants for other steps are omitted for

Received: September 15, 2014
Published: January 9, 2015

DOI: 10.1021/ar500340a
Acc. Chem. Res. 2015, 48, 457−465

clarity. The transition E′ → E may be bimolecular, in which binding of an allosteric regulator shifts the equilibrium from inactive to active states. If some states E′ are not completely inactive, then total reactivity is averaged over multiple (partially) active conformations (not shown). Product release might involve multiple release steps for products and cofactors. Proteins are not single unique structures but interconvert over time scales from femtoseconds to seconds or longer between thermodynamically allowed alternate conformations. NMR spectroscopy allows detailed characterization of the extent and time scales of protein conformational fluctuations linked to numerous stages of complex enzymatic reaction mechanisms, such as that shown in eq 1.

NMR SPECTROSCOPY

NMR spectroscopic phenomena sensitive to time-dependent structural changes in proteins include laboratory frame spin relaxation,[1] relaxation dispersion or line shapes,[2,3] paramagnetic relaxation enhancement (PRE),[4] residual dipolar coupling (RDC),[5] and hydrogen−deuterium exchange (HX).[6,7] This Account focuses on solution NMR laboratory-frame spin relaxation and relaxation dispersion, which uniquely provide information on both distributions of conformations and time scales for interconversion between states.

Laboratory-frame spin-relaxation rate constants most commonly are interpreted using the model-free formalism spectral density function:[8]

$$J(\omega) = \frac{2}{5}\left\{\frac{S^2\tau_m}{1+\omega^2{\tau_m}^2} + \frac{(1-S^2)\tau}{1+\omega^2\tau^2}\right\} \quad (2)$$

in which τ_m is the overall rotational correlation time of the molecule, $1/\tau = 1/\tau_m + 1/\tau_e$, and S^2 and τ_e are the square of the generalized order parameter and effective internal correlation time, respectively, describing the stochastic motions of the principal axis of an axially symmetric interaction tensor in a molecular reference frame. The definition of τ shows that laboratory-frame relaxation is sensitive to processes with $\tau_e \leq \tau_m$, typically picosecond−nanosecond for proteins studied by solution NMR spectroscopy. S^2 is a function of the equilibrium distribution of orientations of the interaction tensor in an internal reference frame:

$$S^2 = \frac{4\pi}{5}\sum_{m=-2}^{2} |\langle Y_2^m(\Omega)\rangle|^2 \quad (3)$$

in which $Y_2^m(\Omega)$ are spherical harmonic functions and $\langle\rangle$ denotes an ensemble average over the probability distribution that the principal axis of the tensor is oriented with angles $\Omega = \{\theta, \phi\}$. The order parameter satisfies $0 \leq S^2 \leq 1$, with the limits reached for fully disordered or completely rigid states, respectively.

The model-free formalism and its extensions[9,10] have been widely applied, for example, to dipole−dipole relaxation of ^{1}H, ^{13}C, and ^{15}N spins, in which the dipole tensor is oriented along the bond vector between a pair of covalently bonded atoms (such as the ^{15}N−^{1}H^N amide group in proteins), or ^{2}H spins, in which the quadrupole tensor is oriented along the covalent bond to the ^{2}H atom.[1] Laboratory-frame relaxation rate constants, notably the longitudinal relaxation rate constant, R_1, the transverse relaxation rate constant, R_2, and the heteronuclear Overhauser cross-relaxation rate constant, σ, are linear combinations of $J(\omega)$ at eigenfrequencies ω of the nuclear spin Hamiltonian.[11] Values of the model-free parameters are obtained by numerical fitting of eq 2 to a set of experimentally determined relaxation rate constants.[12]

Kinetic processes on microsecond−millisecond time scales are termed chemical or conformational exchange in NMR spectroscopy and affect resonance line shapes and transverse relaxation rate constants.[2] Line shapes, measured from one- or multidimensional spectra, and relaxation-dispersion measurements, performed using Carr−Purcell−Meiboom−Gill or $R_{1\rho}$ techniques,[3,13] are analyzed using the Bloch−McConnell equations incorporating the resonance frequencies and "exchange-free" relaxation rate constants of spins in the different states and the kinetic rate constants for interconversion between states. One expression for the $R_{1\rho}$ relaxation rate constant for two interconverting states A and B is given by[14,15]

$$\begin{aligned} R_{1\rho} &= R_1\cos^2\theta + R_2\sin^2\theta \\ &= R_1\cos^2\theta + (R_2^0 + R_{ex})\sin^2\theta \\ &= R_1\cos^2\theta + R_2^0\sin^2\theta \\ &\quad + \sin^2\theta p_A p_B \Delta\omega^2 k_{ex}/({\omega_A}^2{\omega_B}^2/{\omega_e}^2 + {k_{ex}}^2) \end{aligned} \quad (4)$$

in which R_1 and R_2^0 are the relaxation rate constants in the absence of chemical exchange, R_{ex} is the exchange contribution to R_2, $\theta = \arctan(\omega_1/\Omega)$ is the tilt angle of the effective field in the rotating frame of reference, ω_1 is the field strength of the spin-locking field applied with radiofrequency ω_{rf}, $\Delta\omega = \Omega_B - \Omega_A$ is the resonance frequency difference for a spin in states with offset frequencies Ω_A and Ω_B, ${\omega_{A,B}}^2 = {\Omega_{A,B}}^2 + {\omega_1}^2$, Ω is the population-averaged resonance offset, ${\omega_e}^2 = \Omega^2 + {\omega_1}^2$, $k_{ex} = k_1 + k_{-1}$, k_1 and k_{-1} are the kinetic rate constants for transition from state A to B or vice versa, and $p_A \gg p_B$ are the site populations of the two states. Relaxation dispersion profiles, obtained by measuring $R_{1\rho}$ as a function of ω_e, potentially yield k_{ex}, p_A, p_B, and $\Delta\omega$; however, if kinetics approach the fast-exchange limit ($k_{ex} \gg \Delta\omega$), then $\omega_A\omega_B/\omega_e \rightarrow \omega_e$ and only $p_Ap_B\Delta\omega^2$ and k_{ex} can be determined. An expression for the free-precession R_2 is obtained by setting $\theta = \pi/2$ and $\omega_A\omega_B/\omega_e = \Delta\omega$:

$$R_2 = R_2^0 + R_{ex} = R_2^0 + p_Ap_B\Delta\omega^2 k_{ex}/(\Delta\omega^2 + {k_{ex}}^2) \quad (5)$$

and is estimated by line shape analysis, extrapolating a relaxation-dispersion profile to the $\omega_e \rightarrow 0$ intercept, or Hahn spin−echo experiments.[2]

APPLICATIONS

Solution NMR studies that illustrate particular steps in the reaction scheme (eq 1) are highlighted for three enzymes, ribonuclease HI (EC 3.1.26.4, RNase H), AlkB (EC 1.14.11.33), and triosephosphate isomerase (EC 5.3.1.1, TIM), that have been studied in my laboratory. Examples of other enzymes that illustrate similar principles include adenylate[16−19] and other kinases,[20−22] chorismate mutase,[23] dihydrofolate reductase,[24−27] HIV protease,[28−30] prolyl isomerases,[31−34] and ribonuclease A.[35] Notably, spin-relaxation techniques have been applied to protein enzyme systems with masses >200 kDa.[36]

Autoinhibition and Allosteric Activation

As shown in eq 1, interconversion between one or more inactive conformations, E′, and the conformation competent for binding substrate, E, determines the equilibrium population of active enzyme. In the simplest model with a single

DOI: 10.1021/ar500340a
Acc. Chem. Res. 2015, 48, 457−465

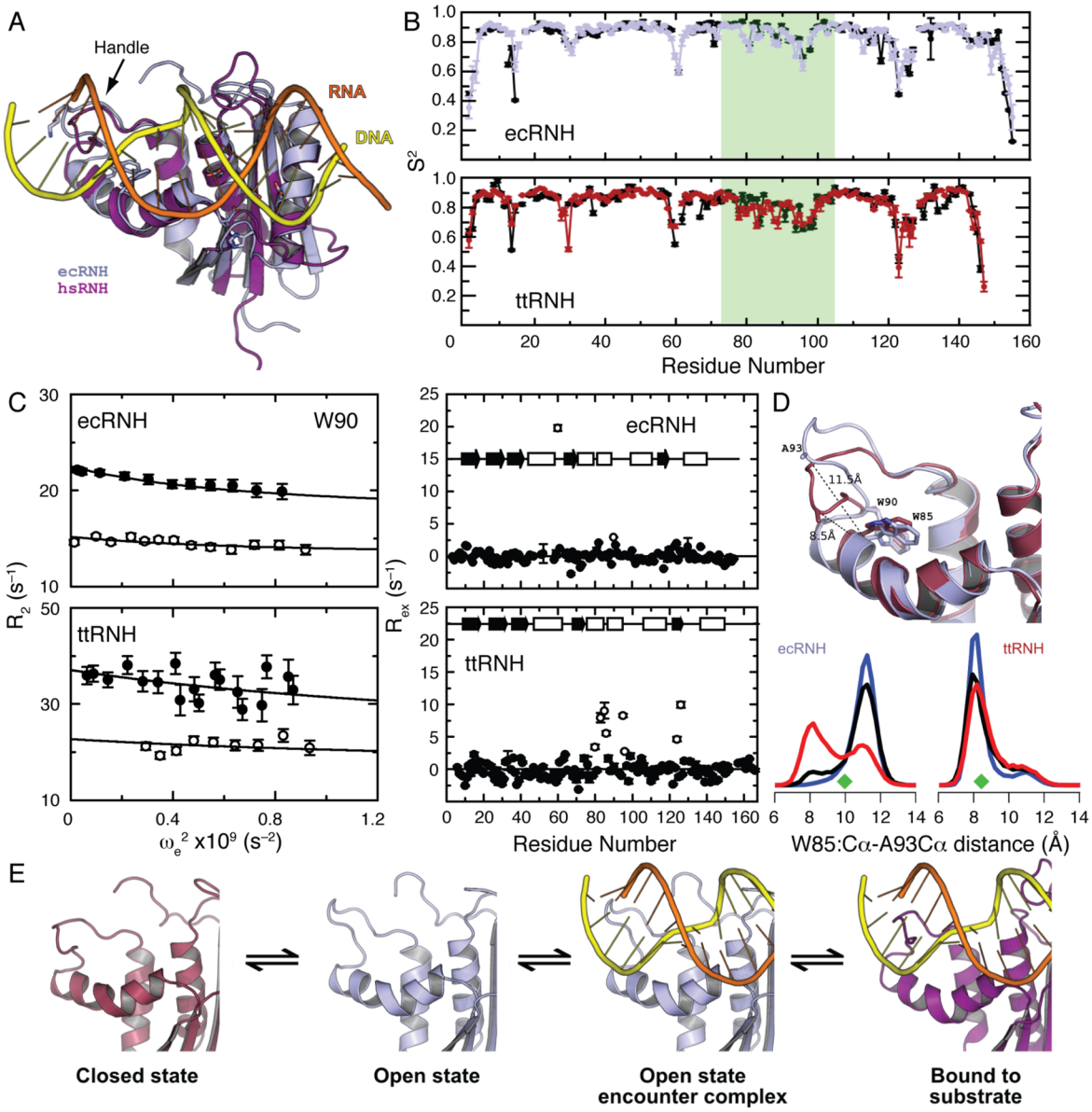

Figure 1. Autoinhibition of RNase H.[38,39] (A) Superposition of the ecRNH structure (light blue, PDB ID 2RN2) with the substrate-bound complex of the hsRNH protein (purple; PDB ID 2QK9), illustrating the position of the handle region interacting with the (yellow) DNA strand of the DNA:RNA hybrid substrate. (B) Backbone amide ^{15}N S^2 (ecRNH residue numbering is used throughout this figure). (top) Experimental (black) and predicted (blue) S^2 for ecRNH. (bottom) Experimental (black) and predicted (red) S^2 for ttRNH. Helices B and C and the handle region are highlighted in green. Experimental values are rescaled by linear regression to the simulated values for visualization. (C) $R_{1\rho}$ relaxation dispersion for backbone amide ^{15}N nuclei. Trp90 $R_2(\omega_e)$ is shown for (top left) ecRNH and (bottom left) ttRNH at 300 K. Closed and open symbols represent data collected at 11.7 and 18.8 T, respectively. Backbone amide ^{15}N R_{ex} at 300 K, 14.1 T for (top right) ecRNH and (bottom right) ttRNH. Values of $R_{ex} \geq 2.5$ s^{-1} are indicated by open circles. (D) (top) Representative conformations from an ecRNH MD trajectory of the (blue) open and (brown) closed states, illustrating the Cartesian W85-Cα–A93-Cα distance metric used to distinguish open (~11.5 Å) and closed conformations (~8.5 Å). The location of Trp90 also is shown. (bottom) Temperature dependence of ecRNH and ttRNH conformational distributions, illustrating the relative populations of the closed and open handle-region states at (blue) 273 K, (black) 300 K, and (red) 340 K. Values of the distance metric from ecRNH and ttRNH (PDB ID 1RIL) crystal structures are shown as green diamonds. (E) Kinetic scheme for the interaction of substrate with the handle region of RNase H, in which the closed and open states are incompetent and competent for binding, respectively. Panel C is from ref 38; other panels are from ref 39.

conformation E′, the apparent Michaelis constant becomes $K'_m = K_m(1 + [E']/[E])$. Thus, increased populations of E′ reduce the apparent affinity of the substrate for the enzyme.

RNase H enzymes are endonucleases that nonspecifically cleave the RNA strand of RNA:DNA hybrid duplex oligonucleotides. Figure 1A shows the X-ray crystal structure of apo *Escherichia coli* RNase H (ecRNH) superposed with the *Homo sapiens* RNase H domain (hsRNH) in complex with substrate. The complex structure identifies three regions important for substrate binding: the loop between β_1 and β_2 (residues 11−22 in ecRNH), α_C and the loop between α_C and α_D (termed the handle region, residues 81−101), and the loop between β_5 and α_E (residues 121−127). Superposition of the holo hsRNH and apo ecRNH structures indicates that all three regions differ in structure between the two proteins, implying

DOI: 10.1021/ar500340a
Acc. Chem. Res. 2015, 48, 457−465

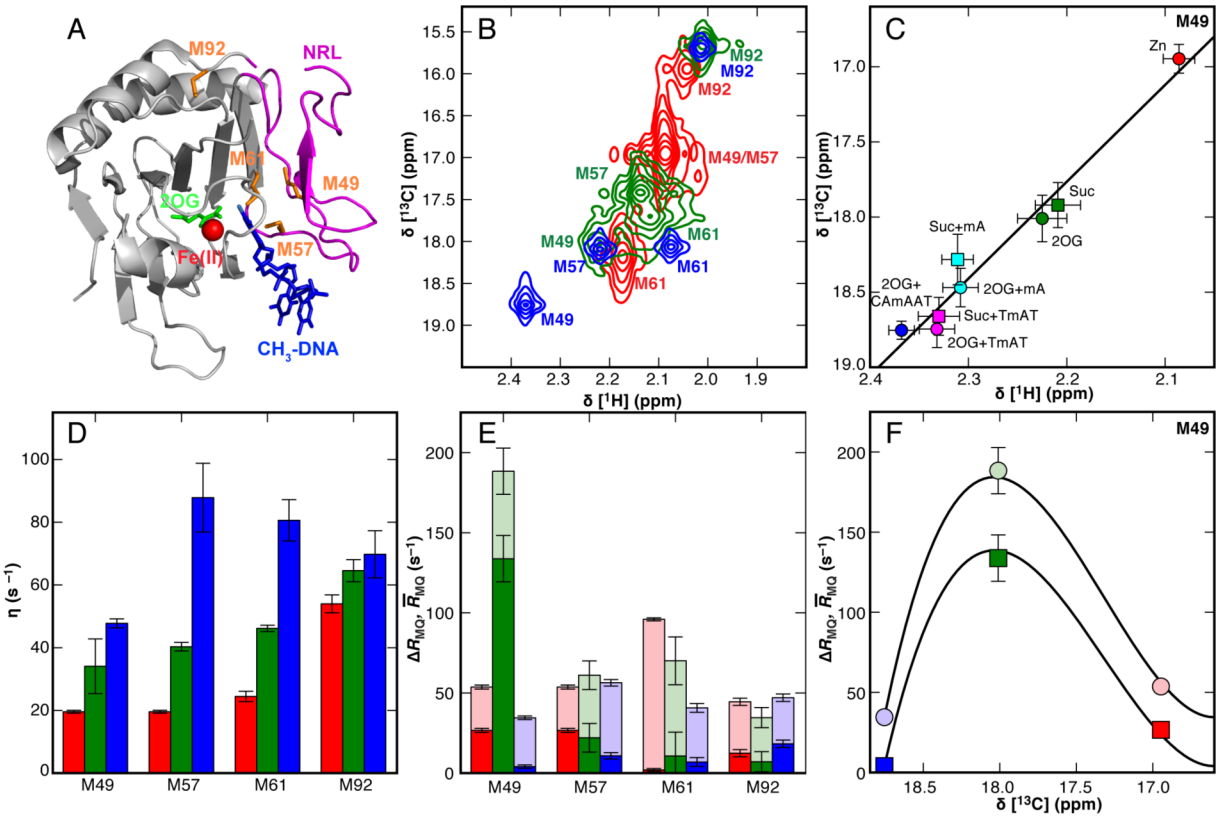

Figure 2. Conformation and dynamics of AlkB characterized by $^{1}H-^{13}C$ NMR at 283 K. (A) X-ray crystal structure of AlkB (PDB ID 2FD8). The Fe(II)/2OG core and NRL are colored gray and magenta, respectively; substrates and cosubstrates (red) Fe(II), (green) 2OG, and (blue) 5′-TmAT-3′ (mA = 1-methyl A) are depicted as spheres and sticks; methionine residues are shown as orange sticks. (B) Methyl $^{1}H-^{13}C$ spectra for $^{13}C^{\epsilon}$-Met AlkB successively titrated with (red) 2.0 × Zn(II), (green) 10.0 × 2OG cosubstrate, and (blue) 1.5 × 5′-CAmAAT-3′ substrate. (C) Linear correlations of the M49 chemical shifts from panel A and from additional spectra of the enzyme saturated with the alternative substrates 1-methyladenosine triphosphate (mA, cyan) or 5′-TmAT-3′ (TmAT, magenta). (D) The methyl $^{1}H-^{1}H$ cross-correlated relaxation rate η. An approximate value $\tau_c = 21.9 \pm 0.5$ ns yields a maximum value of $\eta = 79 \pm 2$ s^{-1} for the closed AlkB/Zn(II)/2OG/5′-CAmCAT-3′ complex. This estimate suggests that M57 and M61 are highly immobilized in the closed complex. (E) (translucent) $\bar{R}_{MQ} = (R_{DQ} + R_{ZQ})/2$ and (solid) $\Delta R_{MQ} = (R_{DQ} - R_{ZQ})/2$ for $^{13}C^{\epsilon}$-Met resonances in AlkB, colored as in panel B. R_{ZQ} and R_{DQ} represent the zero- and double-quantum relaxation rate constants, respectively. (F) Two-state chemical exchange model (solid lines) for (circles) $\bar{R}_{MQ}$ or (squares) $\Delta\bar{R}_{MQ}$. This research was originally published in ref 44. Copyright 2014 American Society for Biochemistry and Molecular Biology.

that conformational rearrangement is required for the bacterial enzyme to achieve a productive enzyme−substrate complex.

A combination of laboratory-frame spin relaxation (Figure 1B),[37] relaxation dispersion measurements (Figure 1C),[38] and molecular dynamics (MD) simulations (Figure 1D)[39] have led to a model for the contribution of the handle region to activity for homologous ribonuclease H enzymes from mesophilic (ecRNH) and thermophilic (*Thermus thermophilus*; ttRNH) bacteria. All three regions involved in substrate recognition show reduced order parameters in the apo enzymes, indicating a broader distribution of amide bond vector orientations on picosecond−nanosecond time scales, compared with elements of secondary structure (Figure 1B). The order parameters are recapitulated in a series of 100 ns MD simulations, which have been independently validated through chemical shift calculations.[40] Relaxation dispersion and Hahn spin−echo experiments (Figure 1C) demonstrate that the handle region of these enzymes undergoes conformational exchange with similar values of $k_{ex} = \sim 4 \times 10^4$ s^{-1}, with the minor state of ttRNH populated at a level ∼3-fold greater than for ecRNH. The NMR experiments, because the exchange process is fast on the chemical shift time scale, do not provide information on the structures of the sparsely populated states. MD simulations (Figure 1D) suggest that the handle region transiently occupies two conformational states. The population distributions derived from MD simulations at three temperatures indicate that the major state is a more open conformation and minor state is a more closed conformation in ecRNH and that the converse is true for ttRNH. These data support a model in which the closed state is inhibitory to binding of substrate. The small fraction of the closed state, ∼1−3%, present at equilibrium of the *E. coli* protein has negligible effect on K'_m, whereas the larger fraction of the closed state, ∼90−97%, present for ttRNH is predicted to increase K'_m substantially, consistent with an ∼8-fold increase in K_m between the ecRNH and ttRNH enzymes at 303 K. Thus, as shown in Figure 1E, substrate forms an initial interaction with the open handle region conformation followed by closure of the loop in a two-step binding process. A subfamily of RNases H, including hsRNH and *Chlorobium tepidum* RNase H, appear to bind substrate in a single step, because altered interactions resulting from a single mutation to aspartate at position 88 props the handle region in a "semi-open" conformation.[39]

Order of Binding Substrates and Cofactors

Enzymes that bind multiple substrates or cofactors may require specific orders of addition, so that S_2 has lower affinity than S_1

DOI: 10.1021/ar500340a
Acc. Chem. Res. 2015, 48, 457−465

to E in eq 1, ensuring that the upper pathway dominates over the lower pathway. If S_2 completely blocks access to the binding site for S_1, the apparent Michaelis constant becomes $K'_m = K_m(1 + [S_2]/K_2)$, in which K_2 is the equilibrium constant for binding of S_2 to E. Consequently, S_2 acts as a competitive inhibitor of the free enzyme E.

Escherichia coli AlkB is an Fe(II)/2-oxoglutarate (2OG)-dependent dioxygenase enzyme that repairs damage to DNA or RNA bases caused by S_N2-alkylating agents.[41,42] The reaction mechanism requires that the cofactor Fe(II) and the cosubstrate 2-oxoglutarate (2OG) bind to the enzyme prior to the alkylated nucleotide primary substrate, as confirmed by X-ray crystal structures in which the bound primary substrate occludes the binding sites for Fe(II) and 2OG (Figure 2A).[43] In the first, oxygen-dependent chemical step, an oxyferryl intermediate is generated by decarboxylation of 2OG to succinate (Suc). The oxyferryl intermediate subsequently hydroxylates the alkyl moiety of the substrate, which spontaneously decomposes after release from the enzyme to recover the unmodified base.

Fluorescence and NMR spectroscopic experiments were used to characterize the mechanism of ordered addition of 2OG and nucleotide substrates.[44] The NMR measurements used the four methionine residues in AlkB as spectroscopic probes, because residues M49 and M57 in the nucleotide recognition lid (NRL) domain and M61 in the dioxygenase core domain are located in the active site in the AlkB/Fe(II)/2OG/5′-TmAT-3′ (mA = 1-methyl A) complex structure (Figure 2A). The fourth residue, M92, is located in a hinge between the dioxygenase and NRL domains. Other studies using backbone ^{15}N NMR experiments have been reported.[45] Titrations performed using Zn(II) as a diamagnetic and catalytically inactive substitute for Fe(II) are shown in Figure 2B. The ^1H and ^{13}C resonances of the terminal methyl group in M49 and M57 exhibit random-coil chemical shifts in the AlkB/Zn(II) complex, suggesting that these side chains are disordered. Addition of 2OG leads to downfield shifts and substantial increases in line widths of both ^1H and ^{13}C resonances. Addition of the 5′-CAmCAT-3′ substrate results in further downfield shifts and dramatic narrowing of the resonance lines, suggesting that the AlkB/Zn(II)/2OG/5′-CAmCAT-3′ complex is highly ordered. The resonances for M61, which is the innermost methionine residue in the active site, display a complex pattern of chemical shift resonance positions, likely from influences of the ligands. The resonances of M92 are only slightly perturbed during the titrations. As shown in Figure 2C, the ^1H and ^{13}C resonances of M49 observed in titrations with a variety of substrates and products are linearly correlated, with longer oligonucleotide substrates yielding more downfield shifts, consistent with increased rigidity. Notably, the M49 and M57 resonances observed in AlkB/Zn(II)/2OG and AlkB/Zn(II)/Suc complexes are intermediate between the AlkB/Zn(II) and AlkB/Zn(II)/2OG/5′-CAmCAT-3′ complexes. The titrations suggest that AlkB/Zn(II) transiently populates a state in which the active site methionine residues (and by extension the NRL) are disordered (termed herein the open state) and a state in which these residues are ordered (termed the closed state).

To confirm this hypothesis, dynamics of methionine $^1H_3{}^{13}C^{\varepsilon}$ groups on picosecond−nanosecond time scales were characterized from the $^1H-^1H$ dipole−dipole cross-correlated relaxation interference rate constant, $\eta \propto S^2\tau_m$.[46] Values of η are small for M49, M57, and M61 of the AlkB/Zn(II) complex, confirming that these side chains are disordered in the open state, and increase first upon addition of 2OG and then upon addition of 5′-CAmAAT-3′ to form the closed complex (Figure 2D). The residues M57 and M61, which are more buried than M49 in the closed complex, have similar η values to M92, which is ordered in all states.

Exchange kinetics between open and closed states were quantified using a methyl TROSY ^{13}C Hahn-echo experiment to measure $^1H-^{13}C$ zero- and double-quantum relaxation rate constants for methionine $^1H_3{}^{13}C^{\varepsilon}$ groups (Figure 2E).[47] The M49 chemical shift and relaxation data were fit simultaneously to a two-site exchange model analogous to eq 5 in the limit $k_{ex} \gg \Delta\omega$, and $\Delta\omega$ refers to differences in zero- or double-quantum frequencies in the two states (Figure 2F). The rate constant for transition to the closed state was determined as $k_1 = 12\,700 \pm 200\ s^{-1}$, assumed to be constant. The populations of the closed state were determined to be 0.16, 0.65, and ∼1 in the Zn(II), Zn(II)/2OG, and Zn(II)/2OG/5′-CAmAAT-3′ complexes, respectively.

Thus, AlkB interconverts on the microsecond−millisecond time scale between an open state, in which the active site methionine side chains are disordered on the picosecond−nanosecond time scale, and a closed state in which the methionine side chains are ordered on the picosecond−nanosecond time scale. Titrations monitored by fluorescence spectroscopy reveal that primary substrates cannot effectively bind to the predominant disordered open state of the AlkB/Zn(II) complex. Binding of 2OG increases the population of the ordered state ∼4-fold and accounts for a substantial fraction of the observed increase in affinity of the 5′-CAmAAT-3′ substrate for the AlkB/Zn(II)/2OG complex compared with the AlkB/Zn(II) complex. Furthermore, the oxyferryl intermediate must remain sequestered from water until the hydroxylation reaction is complete to avoid generation of toxic oxygen species. Fluorescence and NMR data confirm that the opening rate of the enzyme−substrate complex and release of the unreacted methylated DNA substrate is slower than hydroxylation.[44]

Rearrangement of Enzyme−Substrate Complex and Product Release

The initial encounter enzyme−substrate complex, denoted ES_1S_2 in eq 1, may rearrange subsequently to a "closed" enzymatically competent state, $(ES_1S_2)^*$. Closure may form important interactions between the enzyme and substrate but also may prevent adventitious side reactions by excluding water from the active site or restricting release of reactive intermediates (as briefly described for AlkB above). As a consequence, product release from the closed enzyme may become (partially) rate limiting for catalysis.

The enzyme triosephosphate isomerase (EC 5.3.1.1, TIM) catalyzes reversible isomerization of dihydroxy-acetone phosphate to D-glyceraldehyde 3-phosphate. X-ray crystal structures show that the major difference between the homodimeric enzyme in apo and liganded states is an ∼7 Å movement of active site loop 6 (residues 167−177 in *Saccharomyces cerevisiae*) between open, in which the active site is accessible to substrate, and closed, in which the active site is occluded, conformations.[48−50] The closed conformation of the enzyme holds the substrate in the proper orientation for reaction and prevents loss of the enediol reaction intermediate, which otherwise would decompose in solution yielding the toxic product methyl glyoxal.[51]

DOI: 10.1021/ar500340a
Acc. Chem. Res. 2015, 48, 457−465

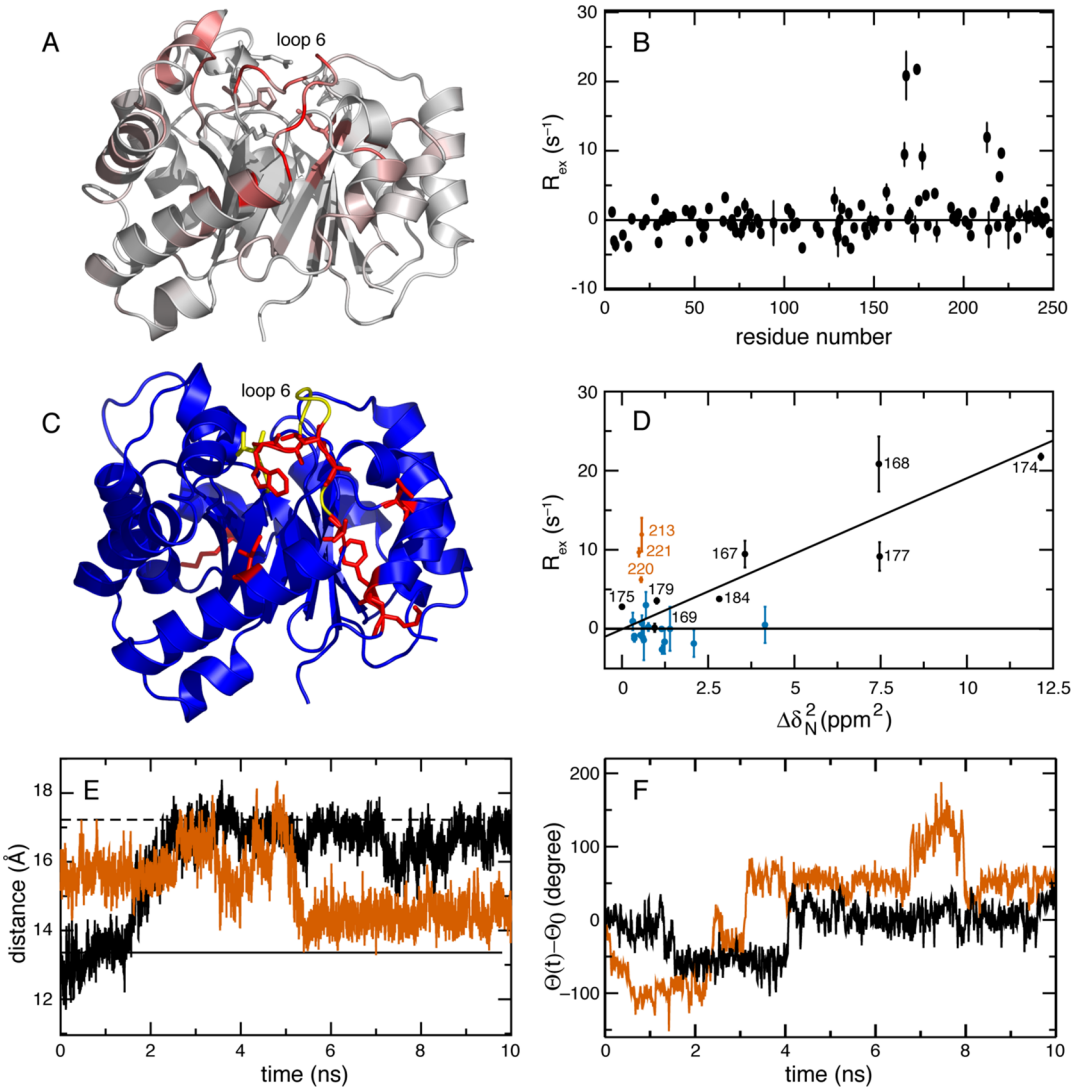

Figure 3. Loop 6 dynamics in triosephosphate isomerase (TIM). (A) ^{15}N ($\Delta\delta_N$) and ^{1}H ($\Delta\delta_H$) chemical shift changes in TIM upon the binding of G3P. The values of $(10\Delta\delta_H^2 + \Delta\delta_N^2)^{1/2}$ are color coded onto the structure of the TIM monomer from white (0 ppm) to red (7.1 ppm). Active site residues Asn10, Lys12, His95, Ser96, Glu97, and Glu165 are shown in stick representation. (B) R_{ex} for G3P-bound TIM at 298 K and 18.8 T. (C) Cartoon representation of the apo structure of TIM; (red) residues with $R_{ex} > 0$, and (yellow) residues located in loop 6 with $R_{ex} = 0$. (D) R_{ex} versus $\Delta\delta_N^2$ at 298 K. A linear correlation is observed for loop 6 residues colored in black (correlation coefficient = 0.9). R_{ex} for (vermillion) residues 213, 220, and 221 is not correlated with loop 6 closing. (blue) Residues that are not part of loop 6 with $\Delta\delta_N^2 > 0$ but $R_{ex} \approx 0$. (E) Distance between the Cα atoms of Gly171 and Y208 monitors loop 6 opening and closing in MD simulations starting from (black) closed (PDB 7TIM) and (vermillion) open (PDB 1YPI) conformations performed at 300 K in the absence of bound ligands. Horizontal lines show the distances in the crystal structures of closed (—) and open (---) states. (F) Cα pseudodihedral angle, Θ, for Gly 173 for trajectories that started from the (black) closed and (vermillion) open states; Θ_0 is the value of Θ in the corresponding X-ray structure. Adapted with permission from ref 52. Copyright 2006 American Chemical Society.

Investigations of loop 6 conformational changes in the W90Y, W157F double mutant of *S. cerevisiae* TIM by solution NMR spectroscopy are summarized in Figure 3.[52] Residues with significant differences in backbone $^{1}H^{N}$ and ^{15}N chemical shift changes between apo TIM and the complex with the substrate analog glycerol 3-phosphate (G3P) interact with or are located near G3P in the active site, with the largest perturbations associated with residues in loop 6 and the following helix F (Figure 3A). Conformational dynamics on microsecond−millisecond time scales were characterized using a TROSY ^{15}N Hahn spin−echo measurement of chemical exchange contributions to transverse relaxation, R_{ex}.[53] Results are shown as a function of amino acid sequence in Figure 3B and are mapped onto the structure of TIM in Figure 3C; large values of R_{ex} are observed for residues in loop 6 and in helix G. Equation 5 indicates that when $k_{ex} \gg \Delta\omega$, a linear correlation is expected for a plot of R_{ex} versus $\Delta\omega^2$ for a set of nuclear spins affected by the same conformational exchange process, that is, the same global kinetic parameters but residue-specific values of $\Delta\omega$. Figure 3D shows a plot of R_{ex} versus the square of the ^{15}N chemical shift perturbation observed upon binding of G3P. The linear dependence for residues in loop 6 confirms that these residues move with the same rate constant, $k_{ex} \approx 3500\ s^{-1}$ at 288 K, and an activation barrier of ~45 kJ/mol, in agreement with solid-state ^{2}H and solution-state ^{19}F NMR spectroscopy of Trp168[54,55] and solution ^{15}N relaxation dispersion measurements.[35]

DOI: 10.1021/ar500340a
Acc. Chem. Res. 2015, 48, 457−465

Stochastic boundary MD simulations with trajectory lengths of 10 ns at 300 K were initiated from both closed and open conformations of TIM, in the absence of any ligands, to confirm and extend the results from NMR spectroscopy. Figure 3E shows the time-dependence of loop motion for residue Gly171 in loop 6; other residues in the loop show similar behavior. If simulations started from the closed conformation of loop 6, then the loop was observed to open during the trajectory. If simulations started from the open state, then the loop sampled closed and open conformations during the trajectory without fully closing. Pseudodihedral angles, Θ, defined between the Cα atoms of $i-1$, i, $i+1$, and $i+2$ were used to quantify local rotational fluctuations of loop 6. Residues i = 166, 174, 175, and 175 at the hinges of the loop exhibit the largest differences in Θ between the X-ray structures of free and bound TIM, while the MD simulations indicate that the most flexible region of the loop is centered around Gly173 (Figure 3F). These results support the conclusion from NMR spectroscopy that loop 6 moves in a correlated fashion and confirm that motions of Gly173 contribute to the initial steps in the opening of the active site loop, required for product release.[56] The MD simulations suggest that the dynamic process in helix G detected by NMR spectroscopy is distinct from the loop 6 motion and may reflect transitions between 3_{10}- and α-helical structures.

CONCLUSION

The above examples have illustrated the application of NMR spectroscopy, often in conjunction with MD simulations, to characterize substrate binding and conformational rearrangements of enzymes at various steps along the reaction scheme shown in eq 1. NMR relaxation methods applied to these examples demonstrate that conformational dynamics on a range of time scales can be associated with autoinhibition and allosteric regulation, substrate recognition, remodeling of enzyme−substrate encounter complexes, and product release. The conformational changes discussed herein for RNase H, AlkB, and TIM do not directly affect the chemical step, k_{cat}. For example, the dramatic difference in rate when the active site loop of TIM is closed reflects the equilibrated enzyme−substrate complex structure, rather than a dynamical effect of the closing loop. In transition state theory, $k_{cat} = (kT/h)C\exp[-E_a/(kT)]$, in which C is a (temperature dependent) prefactor and E_a is the activation energy. Dynamical effects on transition-state barrier recrossing contributions to C (in some reactions quantum mechanical tunneling also contributes to C) have recently been assessed by comparing reactivity in natural abundance and isotopically enriched dihydrofolate reductase.[57] Modern NMR spectroscopy makes extensive use of isotopically enriched proteins and should prove a powerful approach for such investigations in the future.

AUTHOR INFORMATION

Corresponding Author

*E-mail: agp6@columbia.edu. Voice: (212) 305-8675. Fax: (212) 305-7932.

Notes

The authors declare no competing financial interest.

Biography

Arthur G. Palmer, III, received the B.A. in Chemistry from Haverford College in 1980 and the Ph.D. in Chemistry with Nancy L. Thompson from the University of North Carolina at Chapel Hill in 1989. He was a National Science Foundation Postdoctoral Fellow with Peter E. Wright at the Scripps Research Institute from 1989 to 1992. Dr. Palmer joined the faculty of Columbia University as an Assistant Professor in 1992, where he is now the Robert Wood Johnson Jr. Professor of Biochemistry and Molecular Biophysics.

ACKNOWLEDGMENTS

Support from National Institutes of Health Grants GM50291 and GM59273 is acknowledged. Drs. Michelle Gill (National Cancer Institute), Francesca Massi (Univ. Massachusetts Medical School), Mark Rance (Univ. Cincinnati), and Kate Stafford (Univ. California, San Francisco) are thanked for helpful discussions.

REFERENCES

(1) Palmer, A. G. NMR spectroscopy: NMR relaxation methods. In *Biophysical Techniques for Structural Characterization of Macromolecules*; Dyson, H. J., Ed.; Academic Press: Oxford, 2012; Vol. *1*; pp 216−244.
(2) Palmer, A. G. Chemical exchange in biomacromolecules: Past, present, and future. *J. Magn. Reson.* **2014**, *241*, 3−17.
(3) Palmer, A. G.; Massi, F. Characterization of the dynamics of biomacromolecules using rotating-frame spin relaxation NMR spectroscopy. *Chem. Rev.* **2006**, *106*, 1700−1719.
(4) Clore, G. M. Seeing the invisible by paramagnetic and diamagnetic NMR. *Biochem. Soc. Trans.* **2013**, *41*, 1343−1354.
(5) Chen, K.; Tjandra, N. The use of residual dipolar coupling in studying proteins by NMR. *Top. Curr. Chem.* **2012**, *326*, 47−67.
(6) Krishna, M. M.; Hoang, L.; Lin, Y.; Englander, S. W. Hydrogen exchange methods to study protein folding. *Methods* **2004**, *34*, 51−64.
(7) Wildes, D.; Marqusee, S. Hydrogen-exchange strategies applied to energetics of intermediate processes in protein folding. *Methods Enzymol.* **2004**, *380*, 328−349.
(8) Lipari, G.; Szabo, A. Model-free approach to the interpretation of nuclear magnetic resonance relaxation in macromolecules. I. Theory and range of validity. *J. Am. Chem. Soc.* **1982**, *104*, 4546−4559.
(9) Clore, G. M.; Szabo, A.; Bax, A.; Kay, L. E.; Driscoll, P. C.; Gronenborn, A. M. Deviations from the simple two-parameter model-free approach to the interpretation of nitrogen-15 nuclear relaxation of proteins. *J. Am. Chem. Soc.* **1990**, *112*, 4989−4991.
(10) Xia, J.; Deng, N. J.; Levy, R. M. NMR relaxation in proteins with fast internal motions and slow conformational exchange: Model-free framework and Markov state simulations. *J. Phys. Chem. B* **2013**, *117*, 6625−6634.
(11) Cavanagh, J.; Fairbrother, W. J.; Palmer, A. G.; Rance, M.; Skelton, N. J. *Protein NMR Spectroscopy: Principles and Practice*, 2nd ed.; Academic Press: San Diego, CA, 2007.
(12) Mandel, A. M.; Akke, M.; Palmer, A. G. Backbone dynamics of *Escherichia coli* ribonuclease HI: Correlations with structure and function in an active enzyme. *J. Mol. Biol.* **1995**, *246*, 144−163.
(13) Abergel, D.; Palmer, A. G. On the use of the stochastic Liouville equation in NMR: Application to $R_{1\rho}$ relaxation in the presence of exchange. *Concepts Magn. Reson.* **2003**, *19A*, 134−148.
(14) Trott, O.; Palmer, A. G. $R_{1\rho}$ relaxation outside of the fast-exchange limit. *J. Magn. Reson.* **2002**, *154*, 157−160.
(15) Miloushev, V. Z.; Palmer, A. G. $R_{1\rho}$ relaxation for two-site chemical exchange: General approximations and some exact solutions. *J. Magn. Reson.* **2005**, *177*, 221−227.
(16) Shapiro, Y. E.; Kahana, E.; Tugarinov, V.; Liang, Z.; Freed, J. H.; Meirovitch, E. Domain flexibility in ligand-free and inhibitor-bound *Escherichia coli* adenylate kinase based on a mode-coupling analysis of ^{15}N spin relaxation. *Biochemistry* **2002**, *41*, 6271−6281.
(17) Wolf-Watz, M.; Thai, V.; Henzler-Wildman, K.; Hadjipavlou, G.; Eisenmesser, E. Z.; Kern, D. Linkage between dynamics and catalysis in a thermophilic-mesophilic enzyme pair. *Nat. Struct. Mol. Biol.* **2004**, *11*, 945−949.

DOI: 10.1021/ar500340a
Acc. Chem. Res. 2015, 48, 457−465

(18) Kern, D.; Eisenmesser, E. Z.; Wolf-Watz, M. Enzyme dynamics during catalysis measured by NMR spectroscopy. *Methods Enzymol.* **2005**, *394*, 507−524.
(19) Henzler-Wildman, K. A.; Lei, M.; Thai, V.; Kerns, S. J.; Karplus, M.; Kern, D. A hierarchy of timescales in protein dynamics is linked to enzyme catalysis. *Nature* **2007**, *450*, 913−916.
(20) Davulcu, O.; Flynn, P. F.; Chapman, M. S.; Skalicky, J. J. Intrinsic domain and loop dynamics commensurate with catalytic turnover in an induced-fit enzyme. *Structure* **2009**, *17*, 1356−1367.
(21) Veglia, G.; Cembran, A. Role of conformational entropy in the activity and regulation of the catalytic subunit of protein kinase A. *FEBS J.* **2013**, *280*, 5608−5615.
(22) Wang, X.; Vallurupalli, P.; Vu, A.; Lee, K.; Sun, S.; Bai, W. J.; Wu, C.; Zhou, H.; Shea, J. E.; Kay, L. E.; Dahlquist, F. W. The linker between the dimerization and catalytic domains of the CheA histidine kinase propagates changes in structure and dynamics that are important for enzymatic activity. *Biochemistry* **2014**, *53*, 855−861.
(23) Pervushin, K.; Vamvaca, K.; Vogeli, B.; Hilvert, D. Structure and dynamics of a molten globular enzyme. *Nat. Struct. Mol. Biol.* **2007**, *14*, 1202−1206.
(24) Boehr, D. D.; Dyson, H. J.; Wright, P. E. Conformational relaxation following hydride transfer plays a limiting role in dihydrofolate reductase catalysis. *Biochemistry* **2008**, *47*, 9227−9233.
(25) Boehr, D. D.; McElheny, D.; Dyson, H. J.; Wright, P. E. Millisecond timescale fluctuations in dihydrofolate reductase are exquisitely sensitive to the bound ligands. *Proc. Natl. Acad. Sci. U. S. A.* **2010**, *107*, 1373−1378.
(26) Carroll, M. J.; Mauldin, R. V.; Gromova, A. V.; Singleton, S. F.; Collins, E. J.; Lee, A. L. Evidence for dynamics in proteins as a mechanism for ligand dissociation. *Nat. Chem. Biol.* **2012**, *8*, 246−252.
(27) Mauldin, R. V.; Sapienza, P. J.; Petit, C. M.; Lee, A. L. Structure and dynamics of the G121V dihydrofolate reductase mutant: Lessons from a transition-state inhibitor complex. *PLoS One* **2012**, *7*, No. e33252.
(28) Torbeev, V. Y.; Raghuraman, H.; Hamelberg, D.; Tonelli, M.; Westler, W. M.; Perozo, E.; Kent, S. B. Protein conformational dynamics in the mechanism of HIV-1 protease catalysis. *Proc. Natl. Acad. Sci. U. S. A.* **2011**, *108*, 20982−20987.
(29) Cai, Y.; Yilmaz, N. K.; Myint, W.; Ishima, R.; Schiffer, C. A. Differential flap dynamics in wild-type and a drug resistant variant of HIV-1 protease revealed by molecular dynamics and NMR relaxation. *J. Chem. Theory Comput.* **2012**, *8*, 3452−3462.
(30) Ishima, R.; Louis, J. M. A diverse view of protein dynamics from NMR studies of HIV-1 protease flaps. *Proteins Struct., Funct., Bioinf.* **2008**, *70*, 1408−1415.
(31) Eisenmesser, E. Z.; Millet, O.; Labeikovsky, W.; Korzhnev, D. M.; Wolf-Watz, M.; Bosco, D. A.; Skalicky, J. J.; Kay, L. E.; Kern, D. Intrinsic dynamics of an enzyme underlies catalysis. *Nature* **2005**, *438*, 117−121.
(32) Bosco, D. A.; Eisenmesser, E. Z.; Clarkson, M. W.; Wolf-Watz, M.; Labeikovsky, W.; Millet, O.; Kern, D. Dissecting the microscopic steps of the cyclophilin A enzymatic cycle on the biological HIV-1 capsid substrate by NMR. *J. Mol. Biol.* **2010**, *403*, 723−738.
(33) Namanja, A. T.; Wang, X. J.; Xu, B.; Mercedes-Camacho, A. Y.; Wilson, B. D.; Wilson, K. A.; Etzkorn, F. A.; Peng, J. W. Toward flexibility-activity relationships by NMR spectroscopy: dynamics of Pin1 ligands. *J. Am. Chem. Soc.* **2010**, *132*, 5607−5609.
(34) Kovermann, M.; Zierold, R.; Haupt, C.; Low, C.; Balbach, J. NMR relaxation unravels interdomain crosstalk of the two domain prolyl isomerase and chaperone SlyD. *Biochim. Biophys. Acta* **2011**, *1814*, 873−881.
(35) Loria, J. P.; Berlow, R. B.; Watt, E. D. Characterization of enzyme motions by solution NMR relaxation dispersion. *Acc. Chem. Res.* **2008**, *41*, 214−221.
(36) Shi, L.; Kay, L. E. Tracing an allosteric pathway regulating the activity of the HslV protease. *Proc. Natl. Acad. Sci. U. S. A.* **2014**, *111*, 2140−2145.
(37) Butterwick, J. A.; Loria, J. P.; Astrof, N. S.; Kroenke, C. D.; Cole, R.; Rance, M.; Palmer, A. G. Multiple time scale backbone dynamics of homologous thermophilic and mesophilic ribonuclease HI enzymes. *J. Mol. Biol.* **2004**, *339*, 855−871.
(38) Butterwick, J. A.; Palmer, A. G. An inserted Gly residue fine tunes dynamics between mesophilic and thermophilic ribonucleases H. *Protein Sci.* **2006**, *15*, 2697−2707.
(39) Stafford, K. A.; Robustelli, P.; Palmer, A. G. Thermal adaptation of conformational dynamics in ribonuclease H. *PLoS Comput. Biol.* **2013**, *9*, No. e1003218.
(40) Robustelli, P.; Stafford, K. A.; Palmer, A. G. Interpreting protein structural dynamics from NMR chemical shifts. *J. Am. Chem. Soc.* **2012**, *134*, 6365−6374.
(41) Falnes, P. O.; Johansen, R. F.; Seeberg, E. AlkB-mediated oxidative demethylation reverses DNA damage in *Escherichia coli*. *Nature* **2002**, *419*, 178−182.
(42) Trewick, S. C.; Henshaw, T. F.; Hausinger, R. P.; Lindahl, T.; Sedgwick, B. Oxidative demethylation by *Escherichia coli* AlkB directly reverts DNA base damage. *Nature* **2002**, *419*, 174−178.
(43) Yu, B.; Edstrom, W. C.; Benach, J.; Hamuro, Y.; Weber, P. C.; Gibney, B. R.; Hunt, J. F. Crystal structures of catalytic complexes of the oxidative DNA/RNA repair enzyme AlkB. *Nature* **2006**, *439*, 879−884.
(44) Ergel, B.; Gill, M. L.; Brown, L.; Yu, B.; Palmer, A. G.; Hunt, J. F. Protein dynamics control the progression and efficiency of the catalytic reaction cycle of the *Escherichia coli* DNA-repair enzyme AlkB. *J. Biol. Chem.* **2014**, *289*, 29584−29601.
(45) Bleijlevens, B.; Shivarattan, T.; van den Boom, K. S.; de Haan, A.; van der Zwan, G.; Simpson, P. J.; Matthews, S. J. Changes in protein dynamics of the DNA repair dioxygenase AlkB upon binding of Fe(2+) and 2-oxoglutarate. *Biochemistry* **2012**, *51*, 3334−3341.
(46) Tugarinov, V.; Sprangers, R.; Kay, L. E. Probing side-chain dynamics in the proteasome by relaxation violated coherence transfer NMR spectroscopy. *J. Am. Chem. Soc.* **2007**, *129*, 1743−1750.
(47) Gill, M. L.; Palmer, A. G. Multiplet-filtered and gradient-selected zero-quantum TROSY experiments for $^{13}C^{1}H_3$ methyl groups in proteins. *J. Biomol. NMR* **2011**, *51*, 245−251.
(48) Lolis, E.; Petsko, G. A. Crystallographic analysis of the complex between triosephosphate isomerase and 2-phosphoglycolate at 2.5 Å resolution: Implications for catalysis. *Biochemistry* **1990**, *29*, 6619−6625.
(49) Lolis, E.; Alber, T.; Davenport, R. C.; Rose, D.; Hartman, F. C.; Petsko, G. A. Structure of yeast triosephosphate isomerase at 1.9-Å resolution. *Biochemistry* **1990**, *29*, 6609−6618.
(50) Wierenga, R. K.; Borcher, T. V.; Noble, M. E. M. Crystallographic binding studies of triosephosphate isomerase: conformational changes induced by substrate and substrate-analogues. *FEBS Lett.* **1992**, *307*, 34−39.
(51) Knowles, J. R. Enzyme catalysis - not different, just better. *Nature* **1991**, *350*, 121−124.
(52) Massi, F.; Wang, C.; Palmer, A. G. Solution NMR and computer simulation studies of active site loop motion in triosephosphate isomerase. *Biochemistry* **2006**, *45*, 10787−10794.
(53) Wang, C. Y.; Rance, M.; Palmer, A. G. Mapping chemical exchange in proteins with MW > 50 kD. *J. Am. Chem. Soc.* **2003**, *125*, 8968−8969.
(54) Rozovsky, S.; McDermott, A. E. The time scale of the catalytic loop motion in triosephosphate isomerase. *J. Mol. Biol.* **2001**, *310*, 259−270.
(55) Rozovsky, S.; Jogl, G.; Tong, L.; McDermott, A. E. Solution-state NMR investigations of triosephosphate isomerase active site loop motion: ligand release in relation to active site loop dynamics. *J. Mol. Biol.* **2001**, *310*, 271−280.
(56) Derreumaux, P.; Schlick, T. The loop opening/closing motion of the enzyme triosephosphate isomerase. *Biophys. J.* **1998**, *74*, 72−81.
(57) Luk, L. Y.; Javier Ruiz-Pernia, J.; Dawson, W. M.; Roca, M.; Loveridge, E. J.; Glowacki, D. R.; Harvey, J. N.; Mulholland, A. J.; Tunon, I.; Moliner, V.; Allemann, R. K. Unraveling the role of protein dynamics in dihydrofolate reductase catalysis. *Proc. Natl. Acad. Sci. U. S. A.* **2013**, *110*, 16344−16349.

DOI: 10.1021/ar500340a
Acc. Chem. Res. 2015, 48, 457−465

NOTE ADDED IN PROOF

Work described herein for ribonuclease H enzymes has been extended in Stafford, K.A.; Trbovic, N.; Butterwick, J.A; Abel, R.; Friesner, R.A.; Palmer, A.G. Conformational preferences underlying reduced activity of a thermophilic ribonuclease H. *J. Mol. Biol.* **2015**. DOI:10.1016/j.jmb.2014.11.023.

DOI: 10.1021/ar500340a
Acc. Chem. Res. 2015, 48, 457−465